Journal of Earth Sciences and Geotechnical Engineering, Vol. 9, No. 3, 2019, 1-39
ISSN: 1792-9040 (print version), 1792-9660 (online)
Scientific Press International Limited

Disposal of Radioactive Waste in Abandoned Mines

Viktor Popov[1], Robert Adey[2], Roland Pusch[3] and Jörn Kasbohm[4]

Abstract

Countries using nuclear energy tend to favour disposal of Low-Level and Intermediate-Level radioactive waste in mined repositories consisting of series of tunnels or drifts connected to disposal tunnels at a few hundred meters depth. Abandoned mines can serve as repositories for such waste and the present study indicates that this would be possible also for High-Level Waste in the form of spent reactor fuel. The technique implies encapsulation of such waste in metal canisters surrounded by densely compacted smectite clay in relatively shallow mined repositories as well as in very deep bored holes. Intermediate-Level radioactive waste can be disposed of in caverns in the form of packages of metal containers cast in low-pH concrete and embedded in dense smectitic clay.

Keywords: Low-Level and Intermediate-Level radioactive waste (LLW and ILW), smectite clay, compaction, excavation disturbed zone (EDZ), crystalline rock, numerical modelling.

[1] Ascend Technologies, ac, UK
[2] Computational Mechanics Centre, Southampton, UK
[3] Lulea University of Technology, Sweden
[4] Greifswald University, Germany

Article Info: *Received:* June 5, 2019. *Revised:* August 23, 2019.
Published online: September 10, 2019.

1. Scope of study

Repositories for on-ground- and under-ground disposal of short-lived Low- and Intermediate-Level Radioactive Waste (LLW and ILW) have been proposed and constructed since the fifties and a few repository concepts have been proposed for High-Level Radioactive waste (HLW) like spent nuclear fuel. In the paper we propose ILW and LLW to be placed in large caverns. Focus is on underground storage at moderate to large depth, which requires that the rock mechanical stability is certified and that dispersion of possibly escaping radionuclides is hindered from reaching the biosphere for E4 to E5 years. We consider rock stability and hydrology issues for demonstrating that abandoned mines may well be used for safe ILW and HLW disposal. The fact that rock alone will not provide sufficient isolation of hazardous waste makes it relevant to refer to recent R&D results from investigations of the sealing potential of smectite clay.

2. Available abandoned mines for HLW disposal in Europe

Mines that are technically optional for disposal of solid hazardous waste are numerous in Europe. Table 1 lists major ones in Sweden, Finland, Germany, Great Britain, France, Portugal and Spain, in total around 169.

Table 1: Inventory of abandoned European mines of possible use for disposal of hazardous waste (Popov and Pusch, 2006).

Country	Number	Mineral exploited
Sweden	66	Fe, Cu, Zn. Au, Ag
Finland	14	Fe, Al-Fe, Au, Ni, Zn, Pb, Cu
Germany	13	Pb, Zn, Py, Cu, Zn, Ag, Sn, Fe
Great Britain	5	C, F
France	17	C, Sn, F
Portugal	23	Pb, Cu, Zn, Cu
Spain	15	Zn, F, C
Belgium	16	C

3. Underground disposal of radioactive waste

3.1 Crystalline host rock

Following US principles Intermediate-Level Radioactive Waste (ILW) containing long-lived radionuclides requires the same rigorous isolation from groundwater in the host rock of repositories as HLW waste (Pusch, Yong, Nakano, 2018). In this work the authors follow this principle and suggest that ILW, which does not generate heat, be disposed of in big caverns in abandoned mines together with low-level waste. The authors examine how sufficient isolation can be achieved.

3.2 Structural features controlling permeation and stability of crystalline rock

A generalized rock structure model with 1st, 2nd and 3rd order discontinuities in the form of fracture zones and discrete fractures of different size in crystalline rock is shown in Figure 1, which has equivalents in Spain and Switzerland and are designated according to Table 2. Discontinuities of 1st to 3rd orders can cause difficulties in the construction of repositories by having relatively low shear strength, and by controlling regional and local groundwater flow after closing the repository. Most of them can be identified by drillings and geophysical methods. A structural feature is categorized according to what can be observed or measured, but is often part of a larger and more complex assembly of weaknesses in the rock. The difference in hydrological interaction of discontinuities, including fracture zones, for very deep disposal of HLW in boreholes and for shallow HLW repositories is inferred from the figure.

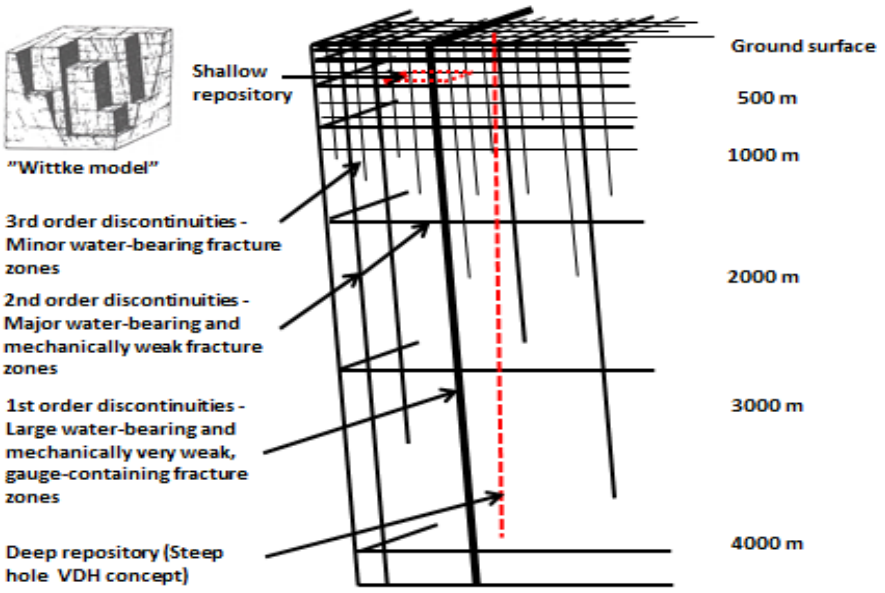

Figure 1: Generalized crystalline rock structure model with fracture zones. The difference between mined (shallow) and deep hole (VDH) repositories is obvious from the different frequencies of intersected weak, water-bearing fracture zones (Pusch et al, 2017).

Table 2: Categorization scheme for rock discontinuities. 1st to 3rd are fracture zones, 4th to 7th are discrete fractures. VH=very high, H=high, M=medium, L=low, VL=very low, VVL=negligible (Pusch, 2008).

Order	Length	Hydraulic conductivity	Gouge content	Strength	D-system (early SKB system)
1st	>Kilometers	VH	VH	VVL	D1
2nd	Kilometers	H	H	VL	D2
3rd	Hundreds of meters	M to H	M	L	D3
4th	Tens of meters	M to H	L	L to MH	D4
5th	Meters	L	VL	MH to H	-
6th	Decimeters	VL	VL	H	-
7th	<Decimeters	VVL	VVL	VH	-

The role of structure in assessing the potential of the host rock to provide mechanical stability of an underground repository is illustrated by the bore profile in Figure 2, which represents the 12 km deep hole bored in Russia (1970 to 1989). The borehole diameter was 214 mm at the ground surface in the Murmansk area, 225 mm at 2,500 m depth and 250 mm at 5,000 m depth. Rock fall had taken place in large parts in the boring process: minor falls had occurred at about 2,500 m depth and more comprehensive falls at 5,000 m depth, and from 6,000 to 9,000 m depth, indicating that they had occurred in fracture zones (NEDRA, 1992). The inner circles represent the intended borehole section and the elongated profile the shape of the actually bored hole. Some of the fracture zones were probably not straight with constant leaning, as indicated by the fact that intersection of the vertical borehole with 250 mm nominal diameter and a 3m wide fracture zone, deviating by 0.02 degrees from the borehole axis, would create a disturbed zone with an axial length of about 80 m.

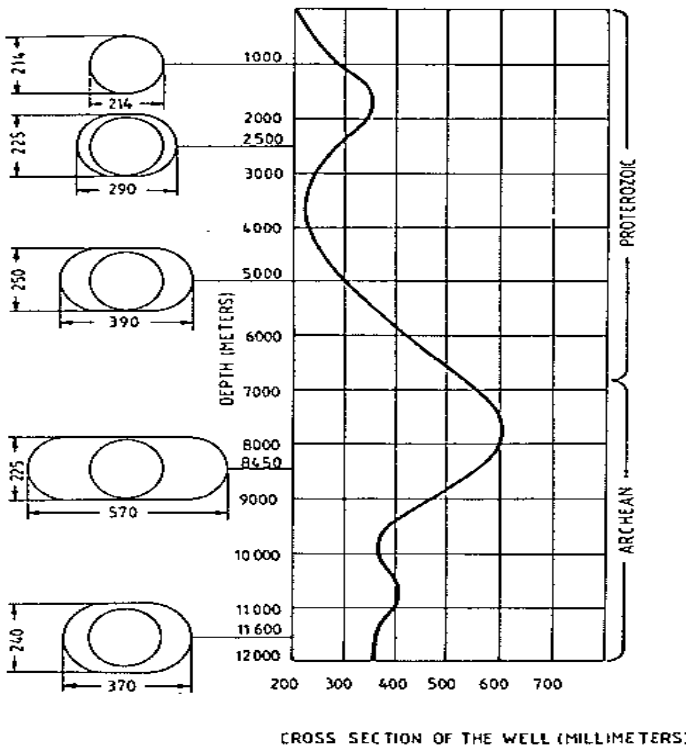

Figure 2: The 12 km deep hole bored in Russia during 1970 to 1989. Minor to more comprehensive rock fall took place in fracture zones at 2,500, 5,000, and 6,000 to 9,000 m depth, indicating that the zones are nearly parallel with the borehole (NEDRA, 1992). The inner circles represent the intended borehole section whilst the elongated profile shows the actual outcome of the boring.

Combination of information gained from empirical structural geology (Anderson, 1951; Milnes, 1998) and theoretical stress/strain analyses has led to models of creation of sills, thrust, strike-slip and dip-slip faults, which later developed to represent all the structural features that one can see today. Figure 3 shows a strain pattern on continental scale caused by large-scale compression and shearing.

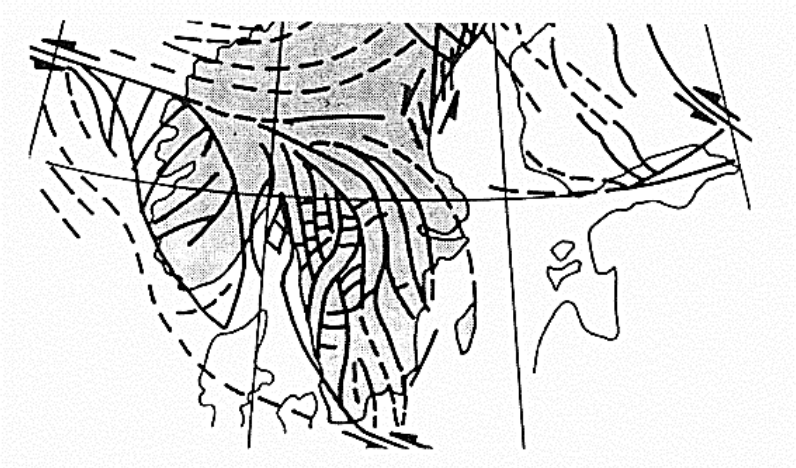

Figure 3: System of large rock discontinuities containing flow paths caused by critically high deviatoric stresses in crystalline rock in southern Sweden (grey). Full lines represent identified features, broken lines show hypothetic ones (After Talbot and Slunga).

Application of basic Rock Mechanics can explain the presence and extension of large structural features as exemplified by Figure 4, which shows a case where sedimentary rock was formed on top of crystalline rock in which high horizontal deviator stresses generated a large-scale Mohr/Coulomb failure pattern. The depth of the trenches indicates the depth of subsequent erosion. Like other ancient shear zones, they are scars with a potential of undergoing further shearing associated with seismic events if they are relatively young and brittle. If they were formed in ancient time, they may represent slow creep strain associated with less dramatic tectonic events.

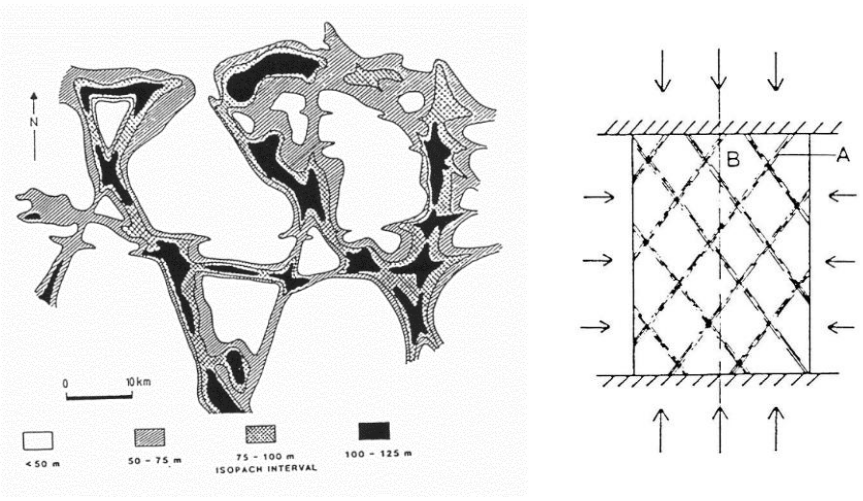

Figure 4: Mohr/Coulomb shear failure modes. Left: Pattern of trenches with indicated depth in sedimentary rock overlying crystalline rock that underwent failure at large-strain caused by high horizontal deviator stresses (After Sanford and Thompson). Right: Large strain causing slip zones (A) but leaving zones in an embryonic failure state in between (B).

Figure 5 shows a sheared zone in crystalline rock illustrating the importance of rock structure for groundwater flow and tunnel stability. The high hydraulic conductivity in the tunnel direction plays a major role for transporting groundwater in the host rock of a repository. The schistosity gives the zone a potential to undergo further splintering and loss in stability if the tunnel is left unfilled for a long time.

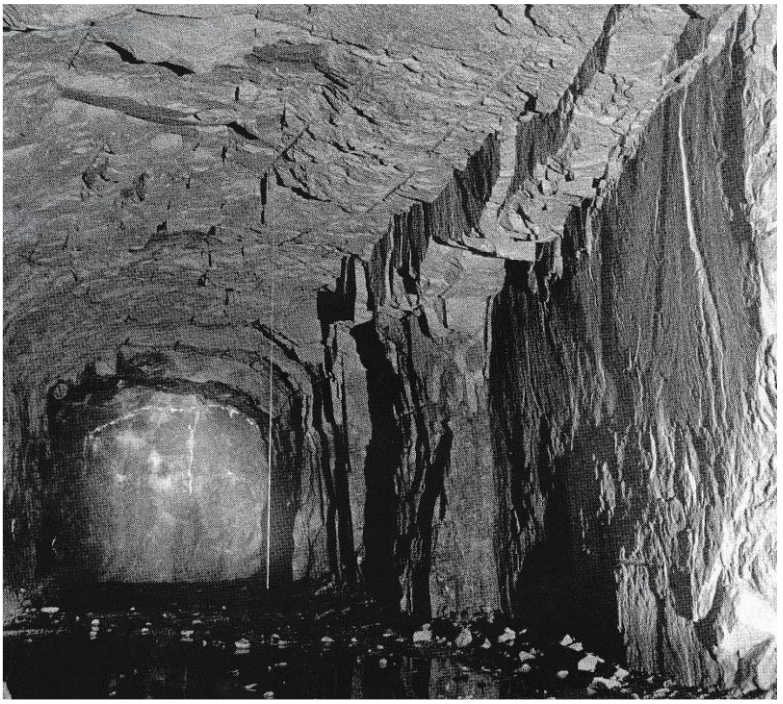

Figure 5: Slabbing and slickensiding caused by large shear strain can give the rock mass strongly anisotropic hydraulic and mechanical properties (After Morfeldt).

Sets of large structural weaknesses are often superimposed by other, more or less orthogonally grouped sets, suggesting that they were formed by rotation of the horizontal stress field and triggered when the orientation generated critically high local stresses at the contacts between displaced blocks, causing rich fracturing as indicated in Figure 6.

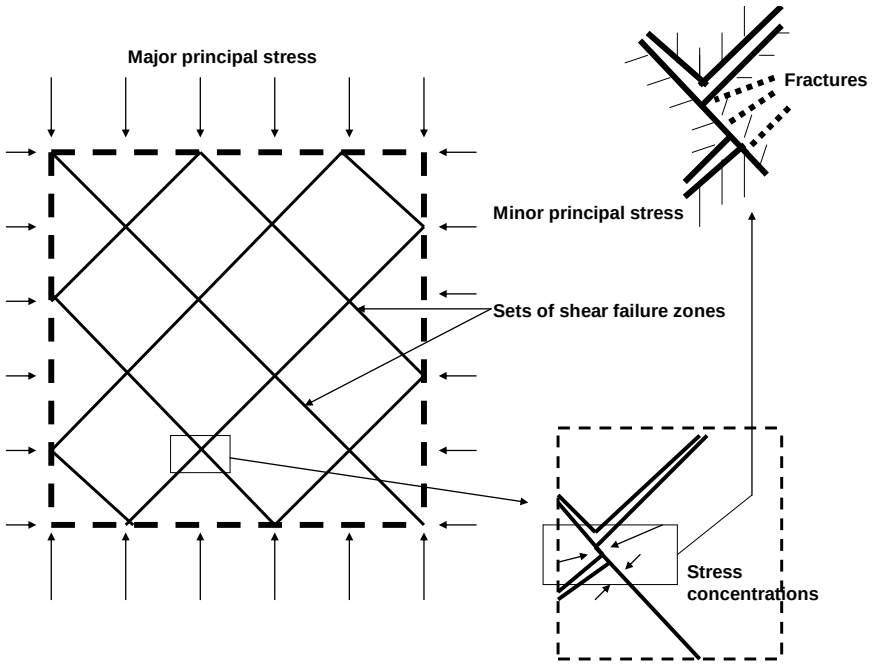

Figure 6: Local high stress concentration at the contacts of big blocks in a rock mass exposed to deviatoric stress conditions leads to "fracture domains" and strongly varying rock pressure (After Pusch).

Naturally, one would like to have straight deposition and transport tunnels for easy and safe waste transport from underground encapsulation stations to deposition holes in repositories, and for rational movement and placement of big boring machines and equipment for installation of waste containers. This is often impossible because of the need to avoid intersection with unsuitably oriented fracture zones. Crossing of systems of parallel deposition tunnels and system of parallel fracture zones can create large, channel-like highly permeable rock zones (Figure 7). Zones generated by shearing on any scale represent weaknesses that were formed in ancient time but often appear to undergo further deformation driven by deviator stresses. Radioactive waste should naturally not be disposed of in such discontinuities, which are of 1st to 3rd orders.

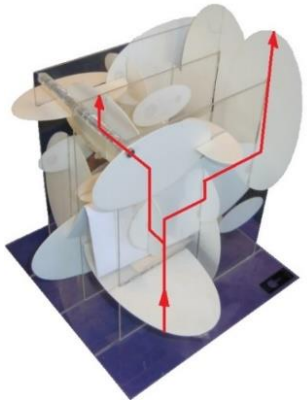

Figure 7: Interacting fractures forming pipe-like channel system.

4. Mine disposal concepts

4.1 Waste types

A condensed summary of IAEA's and national definitions of radioactive waste is shown in Table 3.

Table 3: Definition of radioactive waste for final disposal (*)

Waste classes	Characteristics	Disposal options
1. Exempt waste (EW)	Activity levels at or below clearance levels representing an annual dose of members of the public of less than 0.01 mSv	No radiologic restrictions
2. Low and intermediate waste (LLW/ILW)	Activity levels above clearance levels as defined under (1.) and thermal power below 2 kW/m^3	No radiologic restrictions
2.1 Short-lived waste (LLW/ILW)	Restricted long-lived radio-nuclide concentrations	Near-surface or geologic disposal facility
2.2 Long-lived waste (LLW/ILW)	Long-lived radionuclide concentrations exceeding limitations for short-lived waste	Geologic disposal facility
3. High-level waste	Thermal power above 2 kW/m^3 and long-lived radio-nuclide concentrations exceeding limitations for short-lived waste (Later adjusted)	Geologic disposal facility
(*) IAEA Safety Guide, Classification of radioactive Waste, Safety series No. 111-G-1.1, Vienna (1994)		

4.2 Basis for prediction of stability and percolation

For deciding whether a given abandoned mine can be used for disposal of radioactive waste with acceptably low pollution of the environment one needs to define and apply predictive models respecting stability and isolation capacity. Parameters defining the conditions for dissemination of pollutants and formulation of the models are:

- Type of waste,
- Types of pollutants and species,
- Concentration of dissolved chemical species,
- Type of mine, topology and geometry,
- Local chemical environment,
- Packaging of waste,
- Geology, rock structure,
- Groundwater flow, and pressure gradients

The sections in Figure 8 illustrate the major components of a mined repository in crystalline rock for high-level (HLW), Low-Level (LLW), and Intermediate-Level (ILW) radioactive waste, i.e. 1) host rock, 2) waste containers, 3) engineered barriers made of clay or concrete, and 4) far-field environment. The waste packages in the upper right picture are installed parallel with placing and compacting moderately smectite-rich granular clay (left pointer) and tightly fitted dense liner clay blocks (lower right pointer). The upper right pointer indicates shotcrete of low-pH concrete for smoothening the irregular rock surface. The liner blocks consist of smectite-rich clay (“bentonite”; Pusch, 2017).

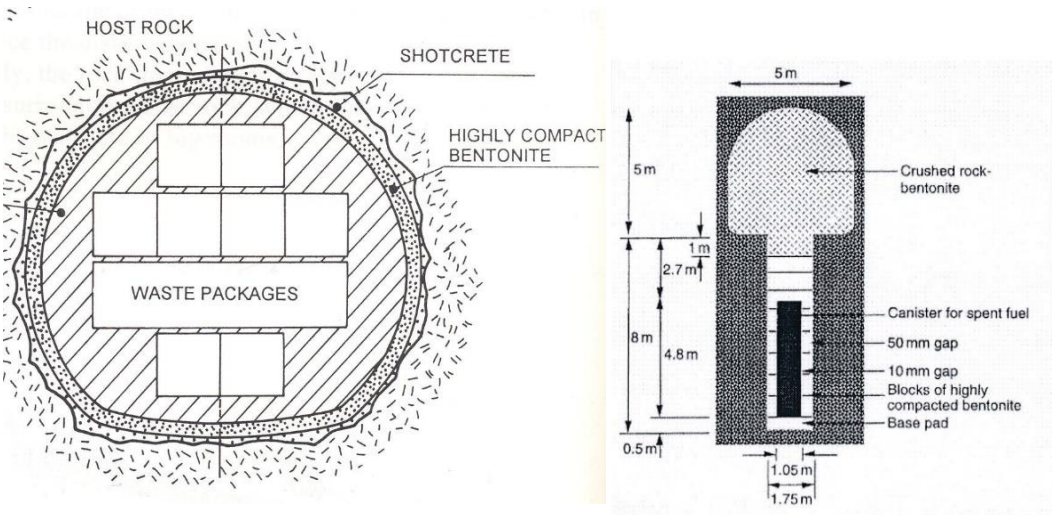

Figure 8: Two repository concepts showing the entities that determine stability and risk of pollution. Upper left: The KBS-3 concept for disposal of HLW in copper/iron canisters surrounded by dense blocks of smectite-rich clay. Lower left: Placement of 2,000 kg clay block. Upper right: disposed LLW or ILW cast in concrete and embedded in effectively compacted granular smectitic clay. Lower right: On-site compacted granular smectitic clay before final rounds by ordinary rollers (Pusch et al, 2017).

4.3 Stability of crystalline host rock

4.3.1 Modelling of the mechanical performance of crystalline rock

Various parameters used in rock stability and flow calculations have been proposed and used. Here, we use those given in Table 4, which have been utilized in the EU projects CROP and LRDT, completed in year 2006.

Table 4: Typical physical properties of discontinuities and rock matrix for crystalline rock. R4, R5 and R6 refer to rock matrix with discontinuities finer than 4^{th}, 5^{th} and 6^{th} orders, respectively.

Rock weaknesses	Hydraulic conductivity, [m/s]	Transmissivity, [m^2/s]	Mohr/Coulomb friction angle, [ϕ^o]	Mohr/Coulomb cohesion, c [MPa]
1^{st} order	E-7 to E-5	E-5 to E-2	15-20	0
2^{nd} order	E-8 to E-6	E-7 to E-4	20-25	0
3^{rd} order	E-9 to E-7	E-9 to E-6	20-30	0
R4	E-11 to E-9	-	20-35	0.1-1
R5	E-12 to E-10	-	35-50	1-10
R6	E-13 to E-11	-	45-60	10-50

Following up the use of effective stress conditions at failure, defined by the Mohr/Coulomb criterion, one can write the equation for the critical state as:

$$\sigma_\iota' = \sigma_\iota + K\,\sigma_3' \qquad (1)$$

where σ_ι' is the major principal stress and σ_3' is the minor principal stress, and K is a multiplication factor for the latter:

$$K = [(1+\sin\phi)/(1-\sin\phi)] \qquad (2)$$

where ϕ is the angle of internal friction.
The unconfined compressive strength is:

$$(2c_o \cos\phi)/(1-\sin\phi) \qquad (3)$$

where c_o is the cohesion intercept.

One needs to consider the zone of excavation disturbance which extends from the periphery of blasted tunnels by 0.25-1.0 m in the walls and by 0.5-2.2 m in the floor depending on the explosive charge and spacing of blast-holes as well as on the sequence of blasting (Figure 9).

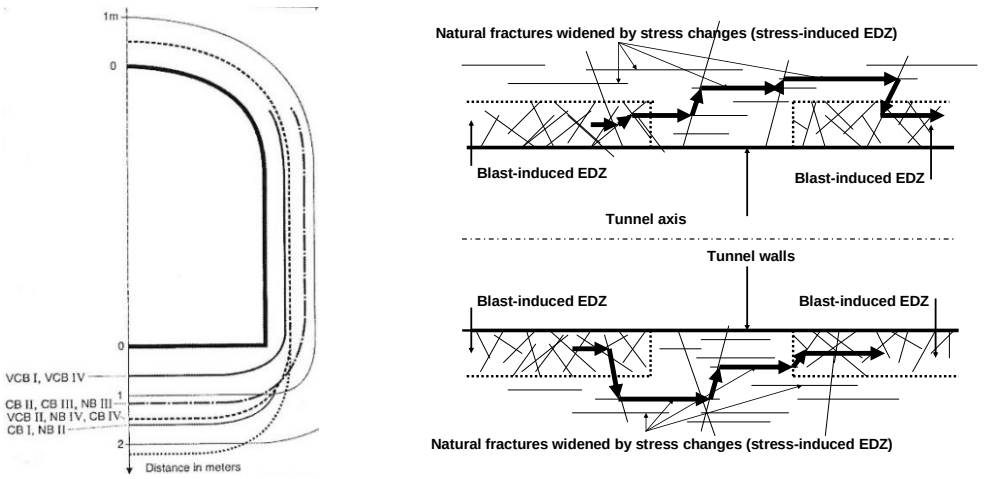

Figure 9: Excavation-disturbed zone (EDZ). Left: Water migration in the zone. Right: Thickness of the zone determined by fracture counting and geophysical measurements. The letter combinations refer to different investigations (Pusch, 1994).

The thickness of the blast-disturbed zone in crystalline rock can be estimated by using data from drillings and seismic measurements as summarized in Figure 9 (right). For modelling of the percolation of groundwater through a repository of the horseshoe type indicated in Figure 8, we will refer to the properties assumed in the EU-project LRDT (Low Risk Disposal Technology) dealing with disposal of hazardous waste. The physical LRDT model had one big room (cavern), for layerwise placed intermediate-level radioactive waste in long-lasting containers and an associated deposition tunnel for placing very hazardous waste, like high-level radioactive waste, in long-lasting canisters (Figure 8). Based on comprehensive structural analyses a basic rock structure model was defined, including discontinuities of 2nd and 3rd orders. The physical properties of these boundaries used in the various modelling attempts in the project are given in Table 4.

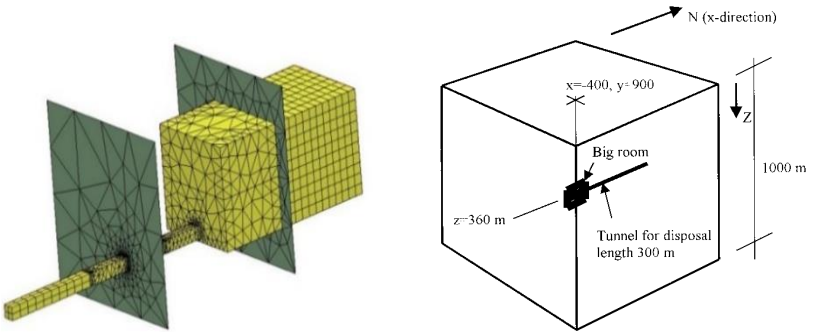

Figure 10: The Stripa cavern and tunnel. The modelled domain includes 1 cubic kilometre of rock with two 3rd order fracture zones. The right picture shows the room and tunnel.

The rock structure model in Figure 10 with all discontinuities grouped orthogonally, adapts in principle to the Stripa region approximately 200 km northwest of Stockholm. The dominant ore was hematite mined from the 15th to the 20th century. The roof of the tunnel has 5 m radius, while the walls are vertical and 5 m apart. The distance between the flat floor and the crown is 5 m. Large-scale ventilation tests and comprehensive packer tests for determining the hydraulic properties of the rock around representative drifts have shown that excavation disturbance extended to 1 m distance from the periphery of the drift (Pusch, 1994). As in all blasted tunnels the resulting excavation-damaged central part of the floor which represents a hydraulically important water conductor that has to be considered in modelling of the hydraulic performance. Figure 11 illustrates a common structure type in Stripa granite in 2D with sets of 4th order discontinuities in the form of fractures and an example of a bored deposition hole in such rock.

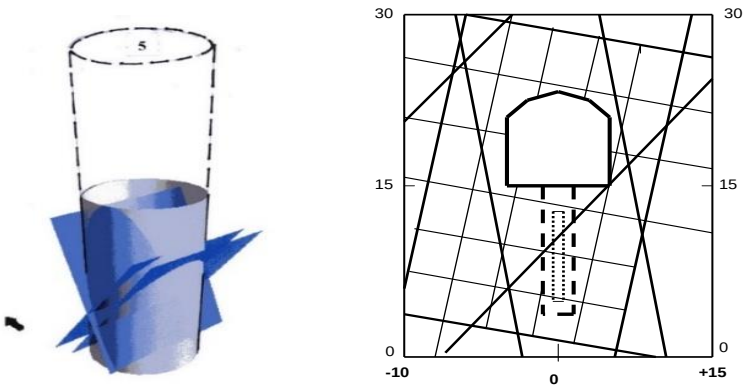

Figure 11: Stripa mine. Left: Generalized structure of the Stripa granite at 360 m depth. Right: Deposition hole with 2 m diameter bored from the tunnel floor is intersected by a few persisting 4th order fractures striking W/E and dipping by 45-60º towards SE or NE.

4.3.2 Modelling of EDZ performance

The Stripa modelling work of to the structural integrity of the repository was based on the Boundary Element code BEASY (Adey and Calaon, 2006) offering a new way of sub-modelling for avoiding numerical problems with the comparatively thin EDZs. This included creation of a series of simplified models with and without the EDZ at the two assumed rock pressures 20 and 30 MPa oriented normal to the vertical symmetry plane. For the lower rock pressure, the walls, the roof and the floor would come under slight tension causing unstable conditions. For the 30 MPa rock pressure the unstable rock volume would be considerably larger.

Calculation of the stress conditions in the tunnel near-field by using the numerical codes UDEC and 3DEC provided the changes in aperture of 4th order discontinuities as demonstrated in Figure 12. It verifies the earlier finding of expansion of fractures in the walls and the EDZs and also of a sub horizontal fracture in the floor, all of which would significantly increase the hydraulic conductivity of the near-field in the direction of the tunnel.

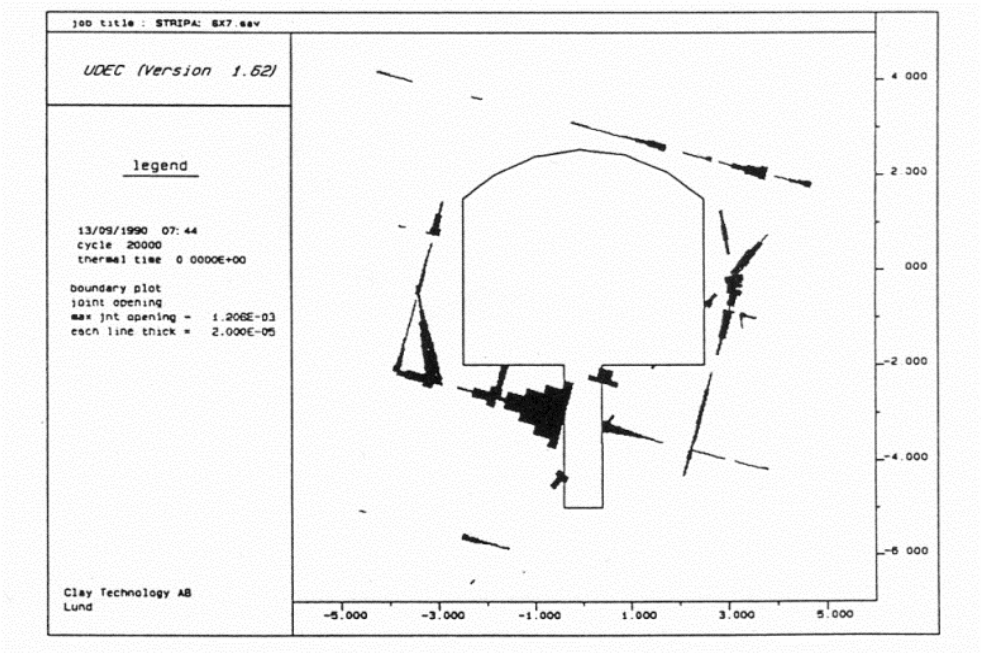

Figure 12: Expansion of fractures around the tunnel and waste-deposition hole in the Stripa mine by creating the open space. Resulting maximum fracture width 1.2 mm (Pusch, 1994).

Similarly, creation of the big room would increase the fracture aperture of a number of natural fractures in the near-field and in the EDZ, which is expected to raise the hydraulic conductivity in the axial direction of the room. The height of it can make the walls unstable, especially where tension stresses prevail, and temporary anchoring by bolting and cement injection may be required. BEM calculations using sub-models showed no practically significant influence of EDZ on the overall rock stability. However, the shallowest part of the EDZ was found to be unstable because of vertical tensile stresses in the high walls of the Big Room. The risk that creep and earthquake vibrations before and after backfilling can widen fractures and soften the EDZ, calls for lining the room with dense clay.

Highly radioactive waste can suitably be placed in bored holes as indicated in Figure 8 and separated from the rock by blocks of expandable clay as indicated in Figure13, while Low- and Intermediate-level radioactive waste with no heat effects after placement, contained in concrete, can be placed in big rooms like the Stripa cavern since there will be no significant difficulties with radiation protection at installation of the waste. The layer-wise placed clay material and waste packages in Figure 13 will, however, need radiation protection in the placement and embedding phases. The waste packages will be embedded in and separated by layers of expansive clay in granular form (“bentonite”) compacted on site.

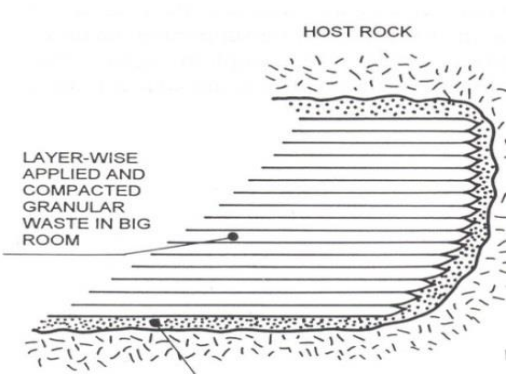

Figure 13: Placed LLW or ILW in a big room, separated by clay in granular form compacted on site. The lower pointer indicates 0.5-1 m of on-site compacted expansive clay and liner blocks of highly compacted smectite clay granules. The clay will ultimately absorb water to 100 % saturation giving it a density of about 1,900-2,000 kg/m^3 (dry density 1,000-1,600 kg/m^3), (Pusch, 1994).

The physical stability of drifts and rooms in abandoned mines intended for disposal of moderately radioactive waste (ILW) depends on the time during which the mine is not yet filled. In ordinary mining, backfilling implies filling drifts and rooms with rock debris that is compressible and with no other impact on the stability than exerting a low earth pressure. For the case of backfilling tunnels and rooms with dense smectitic clay the swelling pressure on the rock will range from some hundreds to a few thousand kPa when the hydration is ultimately complete. This pressure will be sufficient to resist loosening of blocks (Pusch, 1995) and to prevent significant movement of the walls.

For Low- and Intermediate-level radioactive waste the required period of time for effective isolation may be from a few hundred to some thousand years depending on national legislation. A period of this length is sufficient for reaching a high degree of water saturation of the clayey fill in the Big Room and thereby for providing support to its EDZ (Figure 14). After placing the fill, the swelling pressure p will reduce the shear stress and the required compressive strength will drop to σ_z $(1\text{-}k\times p)$ where σ_z is the vertical pressure at the base of the element. For the assumed internal friction angle ϕ=30^o for the EDZ element the required compressive strength will be about 70 % of the vertical pressure. The swelling pressure p hence has a significant stabilizing effect and does not have to be higher than about 0.3 MPa for the Big Room and even less when the mine has ultimately become water saturated.

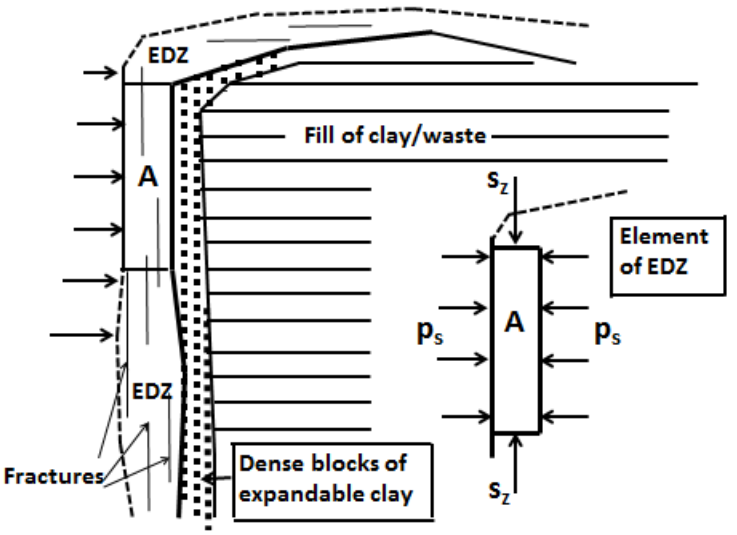

Figure 14: Element of EDZ exposed to an axial pressure s_z caused by gravitation and a horizontal pressure p_S provided by the clay blocks and by the fill. Wall friction between EDZ and intact rock is disregarded.

4.3.3 Saturation of engineered barriers of smectite clay

Placement of waste in mined repositories is made under drained conditions and dispersion of radionuclides by flow and diffusion will not take place until the clay barriers have reached a high degree of water saturation (Pusch et al, 2017). Immediately after closure of a mine repository the groundwater pressure starts to increase by inflow via fracture zones and EDZs, that becomes significant after 50-100 years. Smectite-rich clay barriers are wetted by diffusive water migration rather than by water pressure and various predictions have indicated that the time for complete water saturation can be very long, even longer than the half-life of many radionuclides. The diffusion coefficient is commonly in the interval E-11 m^2/s to E-9 m^2/s (Pusch 2017). The central part of the clay isolation in the big room will hence not have reached a sufficient degree of saturation to initiate migration of radionuclides from leaching canisters and waste containers until several thousand years after closing the mine repository.

4.3.4 Numerical calculation of flow rate

The model referred to here employs two numerical flow models, i.e., a discrete fracture model and an equivalent continuum model (Peratta and Popov, 2006). The discrete fracture model enables one to include the water-bearing discontinuities into the model, which have high impact on the flow and species transport. The equivalent model helps to take into account fractured rock where the fractures are not significant enough to be accounted for separately. A fracture close to a point of interest that would be taken into account as a separate fracture in the model, may be

included in the equivalent continuum model if sufficiently far from the point of interest. In Figure 15, three interacting fractures are shown with their intersections while the rock surrounding the fractures is omitted. The model is three-dimensional (3D) and takes into account the following entities, rock (3D entity in the discrete fracture model taken into account using the equivalent continuum approach), fractures (2D entities in the discrete fracture model), fracture intersections (1D entities in the discrete fracture model), fracture intersections (0D entities in the discrete fracture model).

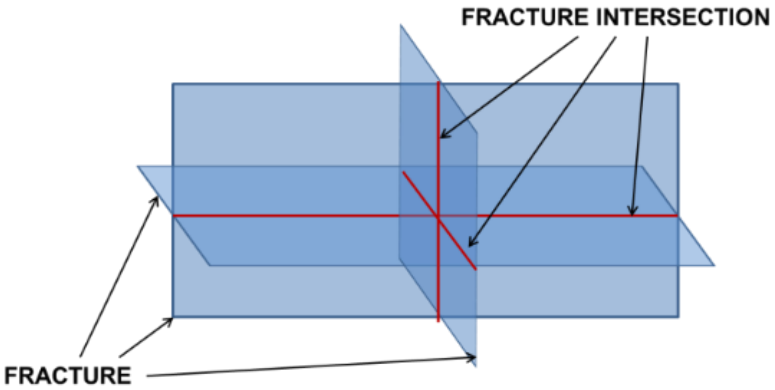

Figure 15: Basic case of fractures forming channels in the rock.

4.3.5 The discrete fracture model

The discrete fracture (DF) model presented here considers the fractured porous media as an incompressible, non-homogeneous mass. Following Peratta and Popov (2006), the equation that describes the transient case of saturated flow in isotropic porous media can be written as:

$$C \cdot \frac{\partial h}{\partial t} + S_{ource} = K \cdot \nabla^2 h \qquad (4)$$

where C is the specific storativity [m^{-1}], h is the hydraulic head [m], K is the hydraulic conductivity [ms^{-1}], t is time [s] and S_{ource} is the source term [s^{-1}].

Equation (3) is valid for porous matrix, fractures and fracture intersections. The interface between two entities is treated in the same way as in any other case of non-homogeneous media (for more information see Samardzioska and Popov, 2005). The flow velocity field is described by the Darcy law:

$$\vec{V} = -K\nabla h \qquad (5)$$

The following equation for transient solute transport is used:

$$\frac{\partial c_i}{\partial t} = \frac{1}{R}\left[\nabla D \nabla c_i - \vec{V} \cdot \vec{\nabla} c_i + \sum_j S_j\right] \qquad (i=1,n) \tag{6}$$

where c_i is the concentration of pollutant *i*, D is dispersion coefficient

$$D = V\alpha + D_m \tag{7}$$

and α is the dispersivity [m], D_m is the molecular diffusion coefficient [m^2s^{-1}], V is the average water velocity [ms^{-1}]. S_j represent sources and sinks of the pollutant and R is retardation factor:

$$R = 1 + \frac{\rho}{\eta} K_D \tag{8}$$

where ρ is the bulk solids density (mass/volume) and η is the porosity. One obtains, for local equilibrium, the surface sorption term K_D as:

$$K_D = \frac{c_i^{soil}}{c_i^{aq}} \tag{9}$$

for the linear portion of the isotherm, and low concentrations, where c^{soil} stands for concentration of species *i* in the immobile solid rock/soil phase, while c^{aq} stands for concentration of species *i* in the mobile aqueous phase.

The first term on the right–hand side of Eq.3 describes the influence of the dispersion on the concentration distribution; while the second term is the change in concentration due to advective transport and adsorption.

4.3.6 The equivalent-continuum model

In the equivalent-continuum (EC) approach, the same equations as for the DF model, (3) and (4) for flow and (5) for solute transport, are used, except that the fractures are not modelled explicitly. In this case they are treated as a continuum with properties derived from an averaging procedure. The hydraulic properties of the domain are averaged over the sub-volume, or representative elementary volume (REV), containing sufficiently large number of fractures.

The equivalent properties used in the present EC model are estimated according to the equations for a simple case of flow through a domain intersected by a family of parallel fractures of equal aperture (see Figure 16 for representation of the geometry and Bear *et al.*, 1993, for theoretical explanation):

- for porosity

$$n_{equi} = n_m \cdot \frac{V_m}{V_t} + n_f \cdot \frac{V_f}{V_t} \tag{10}$$

- for hydraulic conductivity

$$K_{equi} = \frac{\rho \cdot g}{\mu \cdot L}\left(\frac{m \cdot b^3}{12} + k_m \left(L - m \cdot b \right) \right) = K_f \cdot \frac{V_f}{V_t} + K_m \cdot \frac{V_m}{V_t} \tag{11}$$

where n_f and n_m are porosities of the fractures and matrix blocks in the REV, respectively, V_f and V_m are volumes of the fractures and matrix blocks in the REV [m^3], respectively, V_t is total volume of the domain [m^3], L is total thickness of the domain [m], b is aperture of the fracture [m], m is number of parallel fractures, ρ is fluid's density [kg m^{-3}], μ is dynamic viscosity [$kgm^{-1}s^{-1}$], and K_f and K_m are hydraulic conductivities of the fractures and matrix blocks, respectively [ms^{-1}].

The equivalent dispersion coefficient is calculated according to the following expression:

$$D_{equi} = D_m \cdot \frac{V_m}{V_t} + D_f \cdot \frac{V_f}{V_t} \tag{12}$$

where Df, Dm are dispersion coefficients in the fractures and matrix blocks [m^2/s], respectively.

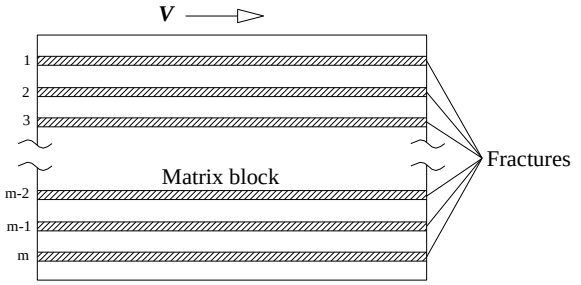

Figure 16: Flow through porous media with parallel fractures used to derive parameters of the EC model.

Although the EC model is commonly employed in describing fractured bedrock, the results obtained represent averaged values over sufficiently large volumes of the domain, implying that it is impossible to have a reliable estimate of the hydraulic head or species concentration in a certain point of the domain. However, for the far field it is sufficient to obtain accurate averaged values of the field variables.

4.3.7 Integration of the entities in the 3D model

Figure 17 shows the way that matrix blocks, fractures and fracture intersections interact. Fractures can be modelled as 2D or 3D entities with certain thickness. The model has been solved by using the boundary element method (BEM), which is particularly suitable for solution of the 3D porous blocks as discretization is required on the surfaces of the porous matrix blocks, which effectively converts 3D into 2D problems Peratta and Popov, 2006.

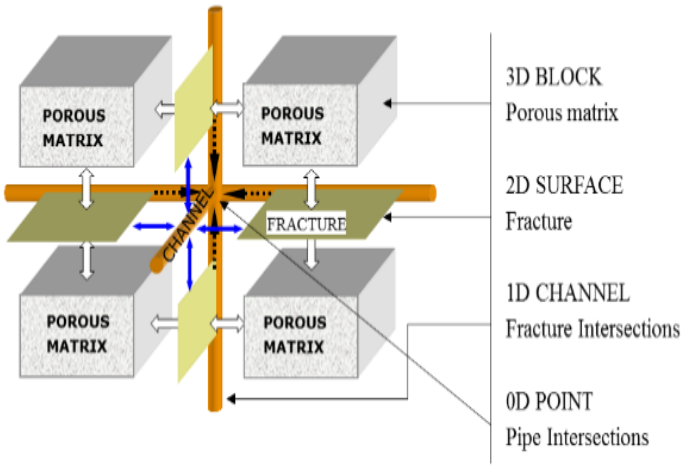

Figure 17: Coupling of matrix blocks, fractures and fractures intersections (channels).

4.3.8 Influence of the EDZ on the flow in the near-field

Full-scale determination of the flow over a 13 m long part of the tunnel was carried out in the Stripa mine (Pusch, 1994) providing the conductivity data shown in Table 5.

Table 5: Evaluated hydraulic conductivity of rock zones; K_r=radial conductivity, K_a=axial conductivity.

Rock	K_a [m/s]	K_r, [m/s]
Undisturbed (virgin)	3E-11 to 9E-11	3E-11 to 9E-11
Stress-disturbed (3-6 m from tunnel)	3E-10 to 9E-10	7.5E-12 to 2.3E-11
Blast-disturbed (0-0.7 m from tunnel)	1.2E-8	1.2E-8

The role of the excavation-disturbed zone (EDZ), which can be taken to have a thickness of 3m around the room and 1m around the tunnel, is particularly important for the groundwater flow in mined drifts and rooms (Pusch, 1994; Pusch et al., 2003). In the present study EDZ was included in the model by considering it as a 2D entity wrapping up the repository. The influence of the EDZ on the flow around a mined repository is demonstrated by the example in Figure 18, in which we recognize the room for storing intermediate-level radioactive waste sandwiched with smectite-rich clay. Three fracture zones intersect the EDZ. The size of the modelled domain was 300m×300m×450m. The hydraulic conductivities used were: 1) for the EDZ: E-7 m/s, 2) for the clay in the sandwiched fill: E-10 m/s, 3) for the undisturbed rock E-9 m/s, 4) for the fracture zones E-7 m/s and 5) for fracture intersections forming channels: 1E-6m/s. These values emanate from comprehensive field measurements

in representative rock volumes of the Stripa mine.
Groundwater flow around the repository is shown in Figure 18(a) for the case with no EDZ included in the model. It can be seen that the velocity field here has a component that is directed away from the room. The reason is the lower permeability inside the room, due to the clay, which diverts most of the flow around the room. The effect of the EDZ is obvious in Figure 18(b) where the flow velocity has a component directed towards the repository. The reason for this is that the EDZ has a higher permeability than the surrounding rock so part of the fluid that would otherwise flow through the surrounding rock is diverted towards this zone that serves as a sink. The continuous EDZ in an underground waste repository hence serves as a major flow path in the repository rock unless it is cut-off by constructing seals in strategic positions (Pusch et al, 2018). These can be constructed by combining on-site cast concrete and plugs of highly compacted blocks of smectite-rich clay.

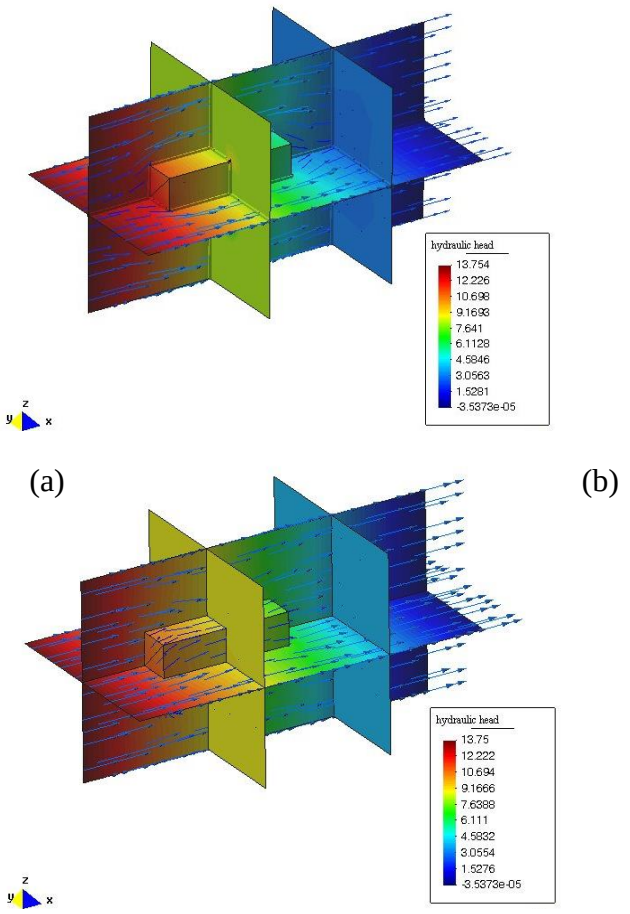

Figure 18: (a) Flow around a room embedded in rock, when the EDZ is not included in the model; (b) Flow around a room embedded in rock with the EDZ included in the model. The prevailing regional hydraulic gradient drives groundwater from left to right.

Typical values of the flow velocity in the rock matrix are two orders of magnitude lower than in the network of fracture zones due to the difference in hydraulic conductivity of the rock matrix and in the backfilled room. The flow is directed towards the EDZ in the inflow part of the EDZ of the room and away from the EDZ/room in the outflow part. This is a consequence of the higher hydraulic conductivity of the EDZ compared to the surrounding rock, making the EDZ responsible for the larger part of the flow in the vicinity of the room.

4.3.9 Contamination of a nearby well

The contamination of the water in a well located 110 m from the end of the tunnel shown in Figure 19, is taken as a measure of the role of the system of discontinuities in distributing the groundwater flow. Pollutants in the form of radionuclides migrating by being transported by water through the repository and the tunnel (left to right in the figure) will be retarded by the low conductivity and ion-absorbing capacity of the clay isolation, which is of the order of 30 mg per 100 g for the mixed-layer smectite/illite Friedland clay. This clay is taken here to represent moderately smectite-rich, commercially available and relatively cheap clays (cf Pusch, 2015)

For determining the degree of contamination of water in the well the source term must be defined and it is taken here as the average concentration of radionuclides at the interface of the clay/EDZ contact, assuming that the water here has reached complete saturation with radionuclides at the start of the groundwater percolation of the big room (10,000 ppm). The total porewater mass in the 50,000 m^3 repository contains 5,000 metric tons of dissolved radionuclides, which represents the worst case scenario when all the waste has been released from the containers at the same time. In reality, the radionuclides will be released from the containers over a long period of time. The total amount of solid clay in the tunnel and room is approximately 100,000 metric tons, the concentration of radionuclides in the big room is hence 5 %.

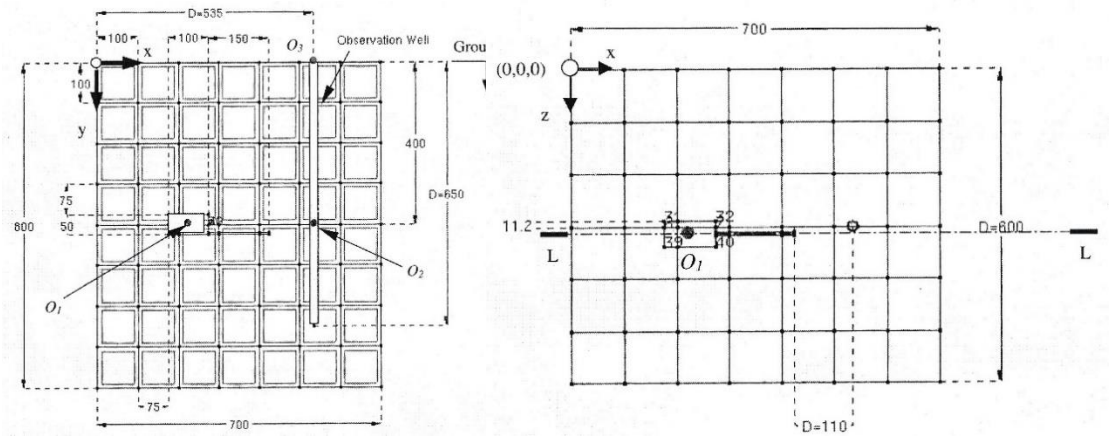

Figure 19: Observation well with 650 m depth drilled in rock with orthogonally grouped 4th order fractures with 5 m spacing, about 300 m from the big room; each block being surrounded by six fractures. Left: Side view, Right: Top view. (After Peratta and Popov, 2006).O_1= geometrical midpoint of the room. O_2= point in the well at room level. O_3= point in the well at ground level.

Following Peratta and Popov it is conservatively assumed that at t = 0 years the clay with adsorbed contaminants is fully water saturated, and that the radioactive matter can travel through the clay into the surrounding EDZ. These investigators used zinc as contaminant while we use radionuclides with corresponding ionic charge.
The sorption coefficient K_d is taken to be 0.02 m^3/kg. Using equation (8) in which ρ is dry density and m the mass of clay one obtains a retardation factor of approximately R = 121. Figure 20 shows the change in time of the concentration of radionuclides in the 400 m deep well.

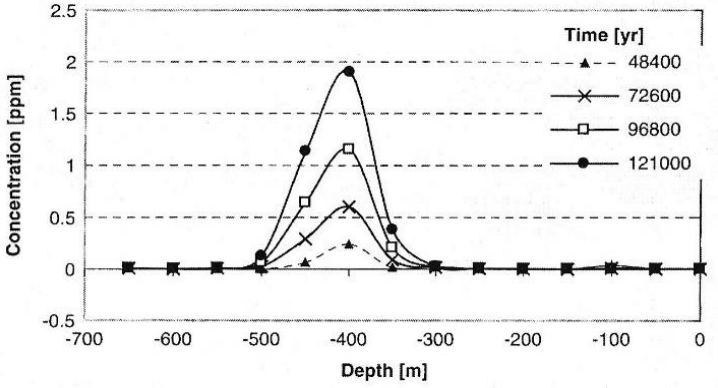

Figure 20: Change in concentration of pollutant in the well water (Peratta and Popov, 2006).

According to Peratta and Popov (2006) the peak concentration in the monitoring well would be reached at 400 m depth after 121,000 years for the considered repository layout and initial conditions. The concentration of pollutants in the well would not exceed 2 ppm, which is much lower than limited by the International Atomic Energy Agency (IAEA) and national authorities. Most of the retardation of the transport of pollutants is due to the sorption into the rock and slow transport through the rock. The short half-life of all radionuclides in LLW and ILW suggests the possibility that they will not have significant impact on the biosphere after a few thousand years. For radionuclides emanating from High-level waste the corresponding time is claimed to be E4 to E5 years.

4.3.10 Chemical aspects

The sealing potential of smectitic clay barriers is largely controlled by the electrolyte content and type of dominant cation in the porewater, which is affected by the composition of the local groundwater (Pusch, 1994, 2015). Swedish investigations have shown that saline conditions with a total content of dissolved salt of 4,000-8,000 ppm and with Na or Ca as dominant cations prevails at 200-500m depth in large parts of Scandinavia and North America. At larger depth than about 500m, the salinity increases but it rarely exceeds that of the oceans above a few thousand meters depth. At about 1,500m depth, the calcium concentration starts to dominate over that of sodium and deeper down the salinity can be very high. Table 6 illustrates the difference in hydraulic conductivity and swelling pressure of smectitic clays in Na and Ca form as function of the density.

Table 6: Geotechnical properties of commercial smectitic clay materials.

Clay mineral type (dominant)	Content of expendables	Dry density, [kg/m^3]	Density at water saturation. [kg/m^3]	K_o/K_s [m/s]	p_o/p_s [kPa]
Montmorillonite	15-25	1,200	1,750	E-10/E-9	20/0
Montmorillonite	15-25	1,650	2,050	5E-11/5E-10	170/10
Montmorillonite	15-25	1,750	2,100	E-11/5E-11	300/30
Montmorillonite	40-60	1,200	1,750	5E-10/E-9	250/50
Montmorillonite	40-60	1,650	2,050	E-12/E-11	1,200/500
Montmorillonite	40-60	1,750	2,100	E-12/5E-12	1,500/1,000
Montmorillonite	70-90	1,200	1,750	E-11/5E-11	1,000/100
Montmorillonite	70-90	1,650	2,050	E-13/5E-13	5,000/3,000
Montmorillonite	70-90	1,750	2,100	E-13/5E-13	10,000/10,000
Saponite	50-60	1,275	1,800	E-12/5E-12	2,500/2,000
Saponite	50-60	1,600	2,000	5E-13/E-12	8,800/5,000
Mx	30-40	1,200	1,750	3E-10/3E-9	50/0
Mx	30-40	1,650	2,050	3E-12/3E-11	1,200/800
Mx	30-40	1,750	2,100	E-12/5E-12	1,500/1,200
In "K_o/K_s" K_o refers to percolation with distilled water while K_s refers to percolation of 3.5% $CaCal_2$ solution. The corresponding meaning is valid for p_o/p_s.					

Clays in Na state hence have significantly lower hydraulic conductivity and higher swelling pressure than equally dense clays in Ca state and one therefore generally uses Na clay as barrier. In shallow mines located in rock with low-saline groundwater such smectite clay barriers retain this state while cation exchange to Ca will take place in deep mine repositories.

Long-term chemical stability of clay barriers is desired and much effort has been put on investigating this matter by oil- and gas production companies, which use clay for sealing prospection and production boreholes. An example of a surprisingly stable smectite clay is a 50 million years old clay from 1,670 m depth below sea bottom in the Oseberg Field in the North Sea, with a content of smectite and mixed layer minerals (S/I) of 66%, which for the estimated temperature of 60 to 80^{o}C, should be about 30 % according to current theoretical models. A typical XRD spectrum for this clay in natural form with and without glycolation and after heating to 350^{o}C and 550^{o}C in the laboratory is shown in Figure 21. A probable explanation of the stability of this clay and of the Swedish Ordovician bentonite (Pusch and Madsen, 1995) is limited access to potassium which underlines the importance of avoiding e.g. potassic ballast in backfills in the repository (cf. Pusch, 2006). It is important to notice that the clay, which is termed claystone, has undergone slight cementation, associated with the illitization.

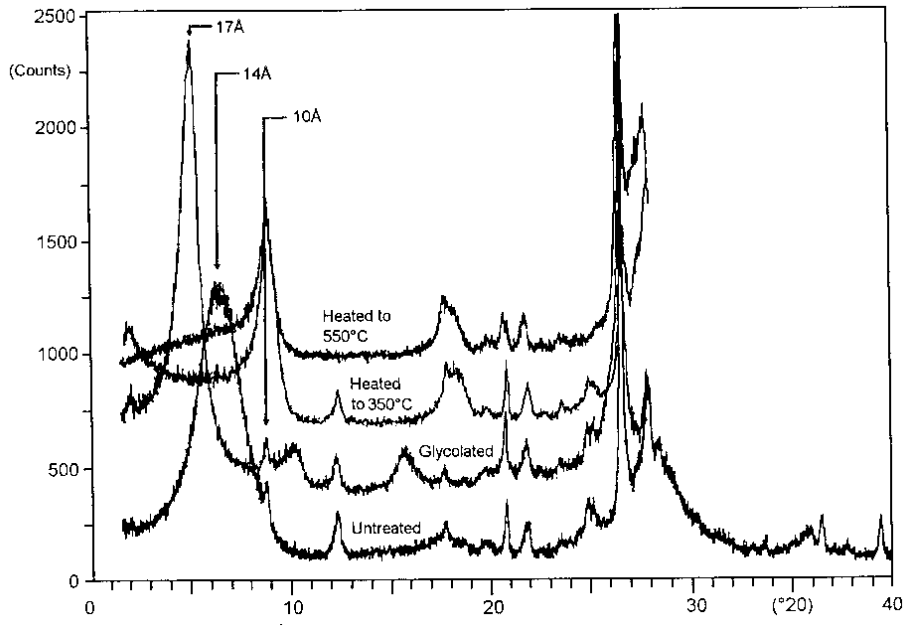

Figure 21: XRD spectrum for a North Sea Tertiary bentonite-type claystone with high content of smectite and high expandability. In most analyses of the natural minus 2 μm fraction a broad 10-14 Å (001) peak was recorded for natural material and this peak changed to 16.9 to 17 Å on glycolation. It collapsed to 10 Å upon heating to 350ºC and higher temperatures (Roaldset et al, 2007).

Processes that can cause degradation of the expanding clay mineral group smectite (cf. Figure 22) to minerals with lower sealing potential, like illite and kaolinite, are:

- Heating to temperatures higher than 60ºC,
- Access to dissolved potassium in the groundwater,
- Precipitation of silicious compounds with silica emanating from partly dissolved smectite clay minerals, feldspars and other Si-bearing minerals.

Hydrothermal tests of smectitic clay and geologic analogies have shown that the crystal structure and content of expandable minerals undergo changes by dissolution, recrystallization and precipitation, for which geochemical models have been worked out by Pytte and Reynolds (1989), Grindrod and Takase (1993) and various other investigators. Systematic hydrothermal testing has been made in France, Germany and the US, as exemplified by numerous series of autoclave experiments conducted at the Geological Department, Texas Tech University at Lubbock, US, using very pure montmorillonite clay (SWY-1) with Al or Fe in octahedral positions in the crystal lattice. These studies are believed to verify the classic alteration mechanism of heat-induced migration of octahedral Al replacing Si in the tetrahedral sheet (Kasbohm et al, 2013). The released silicons together with silicons set free by dissolution of the clay minerals and accessory silicates become

precipitated - "spot-welded" - at the surface of montmorillonite particles which thereby become cemented together (Figure 22).

In France, Germany and Sweden experiments with montmorillonite-rich clay saturated with weakly brackish water, and heated in hydrothermal cells to 130°C at one end and to 20°C at the opposite, have helped to reveal the detailed nature of the degrading processes as illustrated in Figure 23.

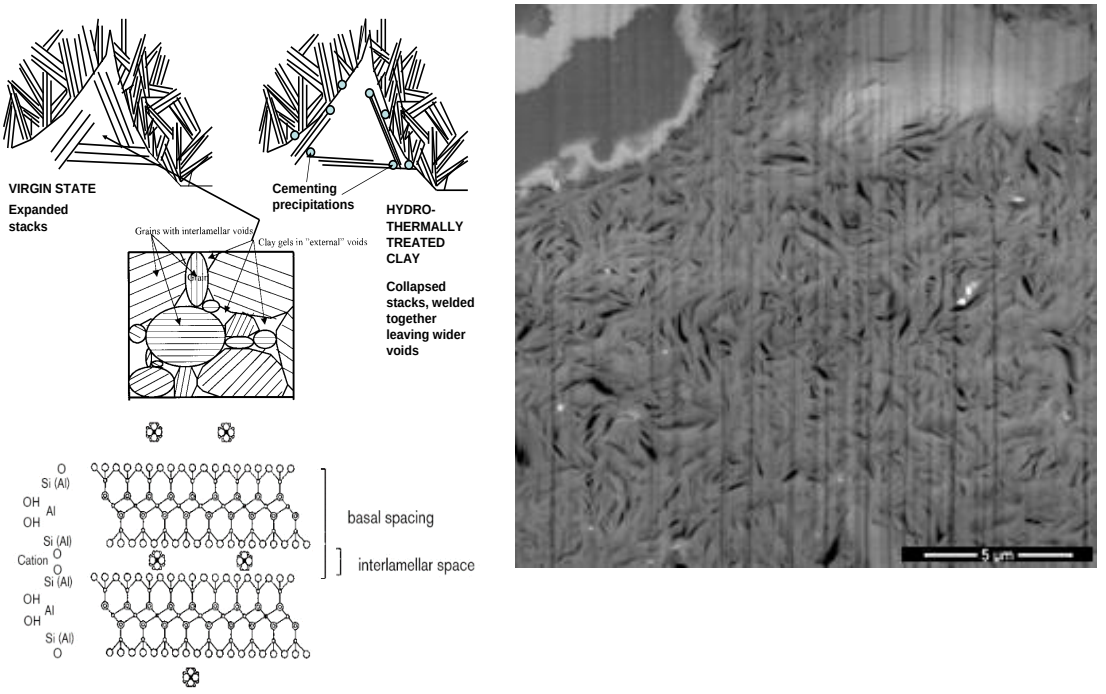

Figure 22: Montmorillonite. Upper left: Proposed thermo-hydro-mechanical-chemical mechanisms affecting the behaviour of smectite clay seals. Lower left: Commonly assumed constitution of stacks of montmorillonite lamellae with 10 Å thickness and hydrated cations in the interlamellar space. Right: Scanning electron micrograph of ion-beam cut sample of montmorillonite clay with 1,300 kg/m^3 dry density after 6 months contact with pH12 concrete, causing ion exchange to Ca and increase in void size (black). (After Warr).

Na ions in the interlamellar space of smectite clays are partly associated with water molecules which can form up to 3 hydrate layers in montmorillonite, while Ca ions can only form 2 hydrate layers. Cation exchange from Na to Ca under constant volume conditions causes microstructural coagulation and increase of the fraction of unassociated water, which raises the hydraulic conductivity. Such microstructural alteration is depicted in Figure 22. Degradation of smectite, which, according to classic clay mineralogy (Pytte/Reynolds, 1989; Grindrod/Takase, 1993; Roaldset et al, 2007) involves reduction of the content of smectite from 100% to about 90% in 1,000 years at 100°C, and further to 35% in 10,000 years, is schematically illustrated in Figure 23. In Figure 24 XRD spectra of natural montmorillonite and of hydrothermally treated clay of the same type exposed to a

temperature gradient of 6ºC/cm, are compared.

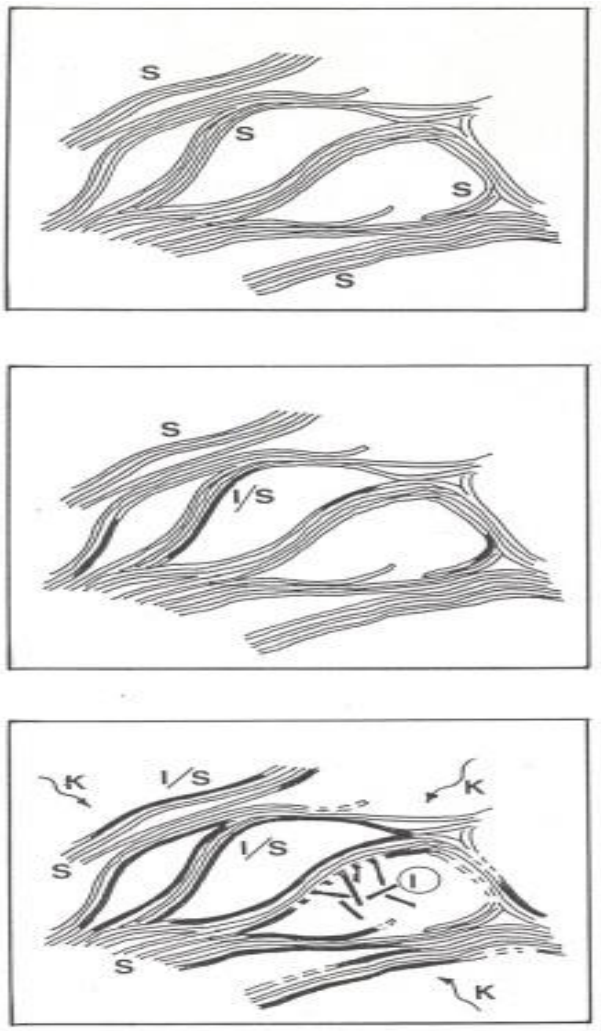

Figure 23: Smectite (S)-to-illite conversion via mixed-layer I/S formation and/or direct precipitation of illite (I). The dark contours represent precipitations of silica and/or illite. (Pusch, 1994).

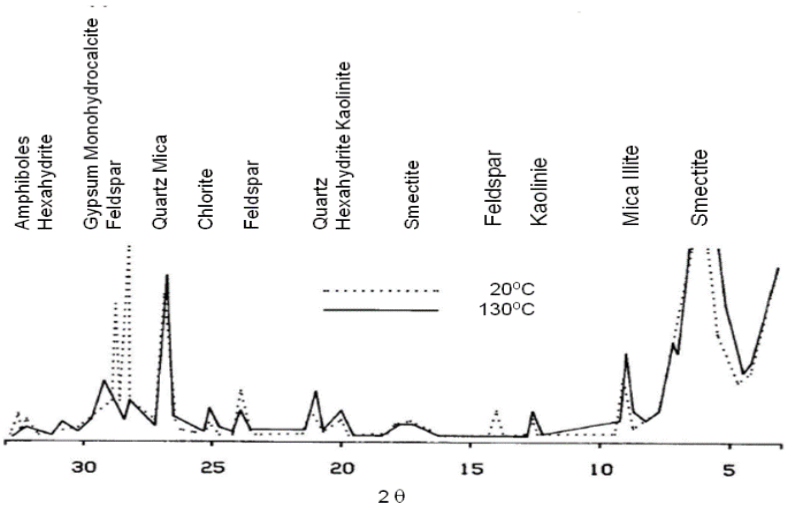

Figure 24: Comparison of rectified diffractograms of montmorillonite-rich clay saturated with weakly brackish water with Na as dominant cation, and heated for one year to 90°C at one end of a hydrothermal cell and to 130°C at the opposite end. Feldspars, amphibole, some of the quartz and smectite disappeared in the hot part (Pusch et al, 1993).

The analyses furthermore showed that strong γ radiation had no impact on the mineral content except that Fe migrated from the iron end plate of the cell into the clay somewhat quicker under radiation. Comparison with virgin MX-80 clay showed that hydrothermal treatment with and without radiation gave insignificant chemical changes, which was also supported by CEC data. They showed that untreated MX-80 had CEC=99 meq/100 g while the most strongly heated and radiated clay had CEC=93 meq/100 g. However, creep testing at room temperature of samples from various distances from the hottest end showed significant stiffening (Pusch et al, 1993). Determination of the shear strain of the sample exposed to 130°C was about 3 times smaller than the one heated to 90°C. Major changes in mineral composition are collected in Table 7; stiffening is obvious from Figure 25.

Table 7: Changes in one year long hydrothermal tests of MX-80. M=Montmorillonite, F=Feldspars, G=Gypsum, Q=Quartz, K=Kaolinite, Chl=Chlorite, I=Illite. +++ means strong increase, ++ significant increase, + slight increase, --- strong loss, -- significant loss, - slight loss. 0 means no change.

Treatment	125-130°C	115-120°C	105-110°C	90-95°C
Hydrothermal without radiation	M - F --- Chl+ G ++ K ++ Q + I +	M – F -- Chl + G +++ K + Q + I 0	M 0 F - Chl 0 G + K 0 Q 0 I 0	M 0 F - Chl 0 G+ K - Q 0 I 0

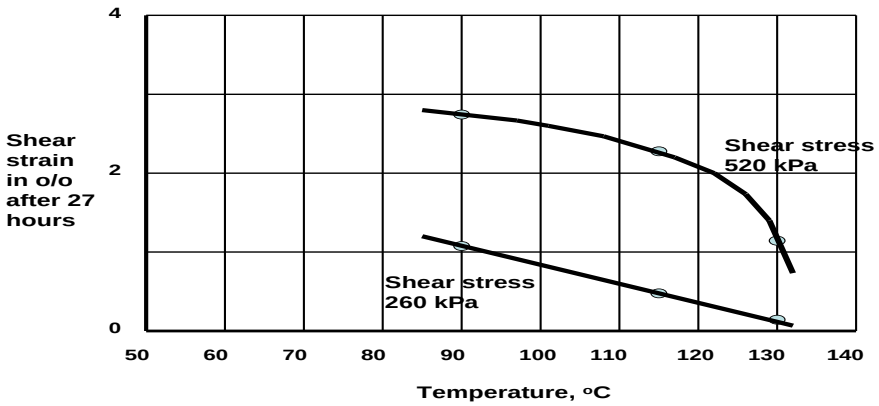

Figure 25: Shear box testing of MX-80 clay from hydrothermal experiment without radiation. Normal stress 6 MPa. The accumulated strain was 2E-4 to 27E-4 in 27 hours (Pusch et al., 1993).

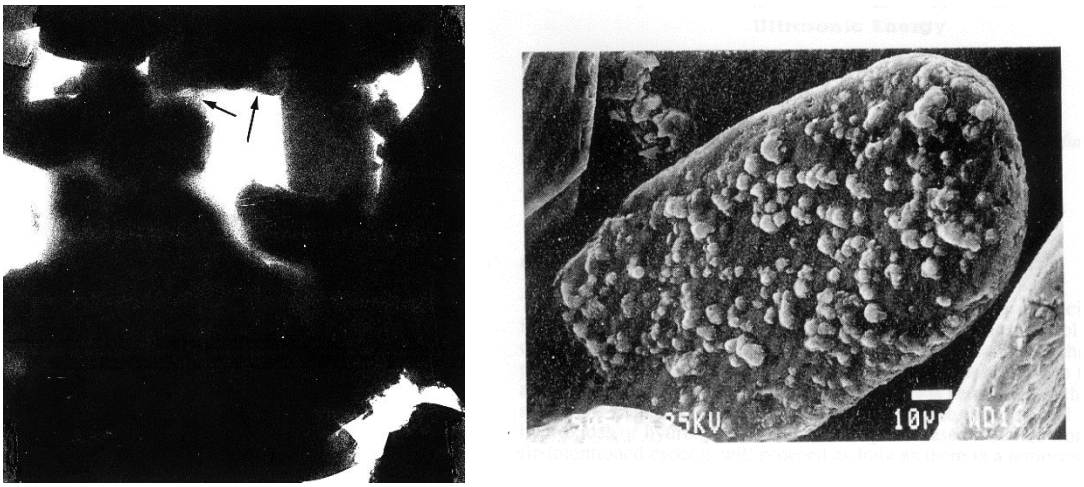

Figure 26: Precipitates in hydrothermally altered smectite clay. Left: Finely porous coatings of clay and silt particles (edge length of micrograph =10 μm). Right: Silica precipitated on silt particle in Ordovician bentonite heated up to about 140°C by intrusion of diabase (After Von-Moos).

The aforementioned thermally generated free silicons together with silicons set free by dissolution of and accessory silicate particles become precipitated as shown in Figure 26, causing significant stiffening and loss of "self-healing" potential as inferred from uniaxial unconfined creep tests (Figure 27).

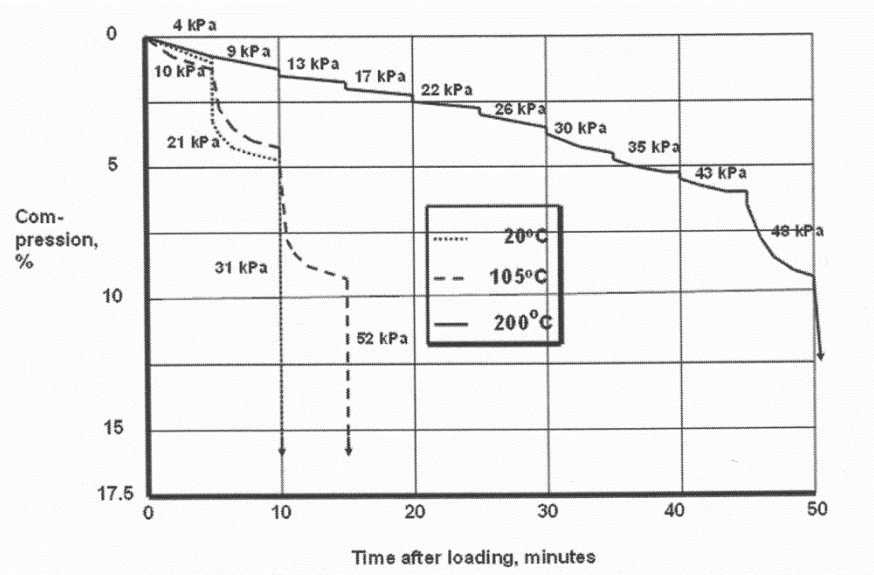

Figure 27: Recorded creep strain by stepwise unconfined loading of samples of smectite-rich clay (MX-80) after hydrothermal treatment at 20ºC, 105ºC and 200ºC for 3 weeks. Some stiffening was found for the 105ºC samples, while heating to 200ºC gave a significant increase in stiffness, loss in creep potential, and ultimately brittle failure. No impact for storage at room temperature was found (Pusch et al, 2011).

5. Construction

5.1 Preparative steps

Establishment of repositories for LLW, ILW and HLW in abandoned mines in crystalline rock primarily requires supporting by bolting and casting of concrete abutments, removal of fallen rock and upgrading of ventilation, railway and electric power systems including lighting. Pipes and drainage systems for pumping off excess amounts of inflowing groundwater and for temporary drainage, must be installed. Access roads to the mine have to be constructed and the entire mine area has to be fenced in and supervised.

5.2 Clay preparation

Smectitic clay for sealing purposes can be prepared by compacting granules delivered by industrial mineral plants for manufacturing blocks or for layerwise placement and compaction. Blocks can be prepared by uniaxial or compression of natural or mixed smectite clays (Pusch, 1994, 2008).

Experience from a number of practical cases of backfilling drifts and rooms underground shows that processing clay by mixing the raw material with sodium carbonate for bringing it in Na form or with other soil material for obtaining a suitable grain size distribution, with subsequent drying, grinding and sieving, is very

expensive and does not always lead to homogeneity. A major issue for organizations like the Swedish Nuclear Fuel and Waste Management has been to work out rational and cheap techniques for finding suitable granular distribution and moisture content. An important conclusion from backfilling of drifts is that natural clay with sufficient smectite content taken directly from stockpiles can be satisfactory after removal of lumps larger than 50 mm, provided that the layers to be compacted are sufficiently thin. Pilot testing should be made by using 420 kg vibrating plates or 7-14 ton vibrating, padfoot and smooth-cylinder rollers (cf. Figure 28). Table 8 exemplifies tests for certifying that compaction by use of vibratory plates and rollers could give the required dry density 1,350 kg/m3.

Figure 28: Vibrating padfoot-roller on compacted natural clay with about 20% water content.

Table 8: On-site compacted layers (10 runs) of natural clay with about 20 % smectite. ρ_n represents the density of the compacted unsaturated clay and ρ_d, represents the dry density.

Layer	Compaction technique	Thickness, [cm]	Density, [kg/m^3], ρ_n/ρ_d	Water content, [%]
1	Vibrating plate 420 kg	11	2,001/1,677	19
2	Vibrating roller, 7 t	17	1,938/1,611**	20
3	Vibrating roller, 7 t	17	1,857/1,583*	17
Base	Concrete floor	>10	2,400	-
* First, bottom layer. ** Second, top layer				

6. Discussion and conclusions

This paper presents current ideas and concepts of disposing radioactive waste in underground mines and the background thereof, including estimation of the mechanical stability of the mine in question, and prediction of the dissemination of leaking radionuclides from waste packages with respect to the isolating capacity of engineered barriers, primarily clay seals. Naturally, any attempt to consider and use abandoned mines for waste disposal must be preceded by legal assurances and an assessment of possible remnants of exploitable ore bodies.

Deep abandoned mines located as far as possible from major rock discontinuities should be considered in the first place since the average hydraulic conductivity drops substantially with increasing depth (Figure 29).

Depth, m	E-14	E-13	E-12	E-11	E-10	E-9	E-8	E-7	E-6	E-5
100										
200										
300										
400										
500										
600										
700										
800										
900										
1000										
1100										
1200										
1300										
1400										
1500										
1600										
1700										
1800										
1900										
2000										

Figure 29: Example of recorded average hydraulic conductivity *K* in m/s in deep boreholes in crystalline rock at Gideå, Sweden. Black represents measured values while red ones are extrapolated.

The conductivity data in Figure 29 represent granite and gneiss, and include those for fracture zones. For 100-200 m depth the average *K* is E-9 m/s. For 300-400 m depth the average *K* is E-10 m/s and for 500-600 m depth *K* is 5E-11 m/s, while for 700-800 m depth the average *K* is E-11 m/s. For 900 to 1500 m depth the average *K* varies between E-13 to E-11 m/s and for 1,600 to 2,000 m depth *K* ranges between E-13 and E-12 m/s. At even larger depth the average *K* is expected to be E-13 m/s or lower. An imaginary repository at 400-500 m depth will be located in rock with an average conductivity of 5E-11 m/s, which is in agreement with the outcome of

comprehensive studies of granite rock like the one carried out as part of the international Stripa Project (Svemar, 2005; Börgesson et al, 1992). These data indicate the advantage of waste disposal rock in deep-bored holes (>2,000m depth; Pusch et al, 2018) where the average hydraulic conductivity is expected to be E-13 to E-11 m/s, i.e. at least two orders of magnitude lower than for a repository at 400-500 m depth.

References

[1] Anderson, E.M. (1951).The Dynamics of Faulting. Hafner, New York, US.
[2] Bear J, Tsang C and Marsily G. (1993). Flow and contaminant transport in fractured rock. San Diego California: Academic Press Inc.
[3] Börgesson, L., Pusch, R., Fredriksson, A., Hökmark, H., Karnland, O., and Sandén (1992). Final Report of the Rock Sealing Project – sealing of Zones Disturbed by Blasting and Stress Release. Stripa Project Technical Report 92-21. Swedish Nuclear Fuel and Waste Company SKB, Stockholm, Sweden.
[4] Grindrod, P. and Takase, H. (1993). Reactive chemical transport within engineered barriers. (In: Proc. 4th Int. Conf. on the Chemistry and Migration Behaviour of Actinides and Fission Products in the Geosphere, Charleston, USA, 12-17 Dec.), Oldenburg Verlag 1994 (773-779).
[5] Kasbohm, J., Pusch, R., Nguyen-Than, L. and Hoang-Minh, T. (2013). Lab-scale performance of selected expandable clays under HLW repository conditions. Environ Earth Sci. DOI 10.1007/s12665-012-20851.
[6] Milnes, A.G (1998). Crustal structure and regional tectonics of SE Sweden and the Baltic Sea. SKB Techn. Rep. TR-98-21. Swedish Nuclear Fuel and Waste Company SKB, Stockholm, Sweden.
[7] NEDRA, (1992). Characterization of crystalline rocks. SKB Technical Report TR 92-39. Swedish Nuclear Fuel and Waste Company, Stockholm, Sweden.
[8] Peratta, A. and Popov, V. (2006). A new scheme for numerical modelling of flow and transport processes in 3D fractured porous media, Advances in Water Resources, 29, 42-61.
[9] Pusch, R., Karnland, O., Lajudie, A. and Decarreau, A. (1993). MX-80 exposed to high temperatures and gamma radiation. SKB Technical Report TR-93-03. Swedish Nuclear Fuel and Waste Management AB (SKB), Stockholm, Sweden.
[10] Pusch, R. (1994). Waste disposal in rock, Dev.in Geotechnical Engineering 76, Elsevier Publ. Co. ISBN: 0-444-89449-7.
[11] Pusch, R. and Madsen, F. (1995). Aspects on the illitization of the Kinnekulle bentonites. Clays and Clay Minerals, 43(3), 261-270.
[12] Pusch, R., Zwahr, H., Gerber and Schomburg, J. R. (2003). Interaction of cement and smectite clay – theory and practice. Appl. Clay Science, Vol.23 (pp.203-210).
[13] Pusch, R., Börgesson, L. and Ramqvist, G. (2003). Hydraulic characterization of EDZ in a blasted tunnel in crystalline rock – measurements and evaluation.

Proceedings of a European Commission CLUSTER conference held in Luxemburg on 3-5 November 2003, 69-76.

[14] Pusch, R. and Yong, R. N. (2006). Microstructure of smectite clays and engineering performance. Taylor & Francis, London and New York.

[15] Pusch, R. (2008). Geological Storage of Radioactive Waste. Springer-Verlag, Berlin Heidelberg.

[16] Pusch, R., Yong, R.N. and Nakano, M. (2011). High-level Radioactive Waste Disposal. WIT Press, Southampton, Boston.

[17] Pusch, R. (2015). Bentonite Clay, CRC Press (Taylor & Francis Group), ISBN 13:978-1-4822-4343-7.

[18] Pusch, R., Yong, R.N. and Nakano, M. (2018). Geologic Disposal of High-Level Radioactive Waste. Taylor & Francis, London and New York.

[19] Roaldset, E., Bjaanes, E. and Mjöen, K. (2007). Stability of smectite – environmental aspects of petroleum geological observations. Workshop on microstructural modelling of natural and artificial smectite clays. IDEON Scientific Park, Lund, Sweden.

[20] Samardzioska, T. and Popov, V. (2005). Numerical comparison of the equivalent continuum, non-homogeneous and dual porosity models for flow and transport in fractured porous media. Advances in Water Resources, 28, 235-255.

[21] Svemar, C. (2005). Cluster Repository project (CROP). Final Report of European Commission Contract FIR-CT-2000-2003, Brussels, Belgium.